Information-based analysis of simple incoherent imaging systems

Amit Ashok and Mark A. Neifeld
Department of Electrical and Computer Engineering
University of Arizona, Tucson, AZ 85721 USA
ashoka@ece.arizona.edu

Abstract: We present an information-based analysis of three candidate imagers: a conventional lens system, a cubic phase mask system, and a random phase mask system. For source volumes comprising relatively few equal-intensity point sources we compare both the axial and lateral information content of detector intensity measurements. We include the effect of additive white Gaussian noise. Single and distributed aperture imaging is studied. A single detector in each of two apertures using conventional lenses can yield 36% of the available scene information when the source volume contains only single point source. The addition of cubic phase masks yields nearly 74% of the scene information. An identical configuration using random phase masks offers the best performance with 89% scene information available in the detector intensity measurements.

OCIS codes: (110.0110) Imaging systems; (200.3050) Information processing; (220.4830) Optical systems design

References and links

1. J. van der Gracht and G. W. Euliss, "Information-optimized extended depth-of-field imaging systems," Visual Information Processing X, 103-112, (2001).
2. M. A. Neifeld, "Information-optimized imaging systems design," Visual Information Processing X, 113-116, (2001).
3. S. Reichenbach, Y. Xiong, R. Narayanan, and L. Cao, "Information theoretic assessment and design of hyperspectral imaging system," Visual Information Processing, Proc. SPIE , **3716**, 100-104, (1999).
4. M. A. Neifeld, "Information, resolution and the space-bandwidth product," Opt. Lett., **23**, 1477-1478, (1998).
5. E. R. Dowski, "An Information Theory Approach to Incoherent Information Processing Systems," http://www.colorado.edu/isl/papers/info/paper.html.
6. F. O. Huck and S. K. Park, "Optical-mechanical line-scan imaging process: Its information capacity and efficiency," Appl. Opt., **14**, 2508-2520, (1975).
7. S. Prasad, "Information capacity of a seeing-limited imaging system," Opt. Comm. , **177**, 119-134, (2000).
8. S. Prasad, "Statistical-information-based performance criteria for Richardson-Lucy image deblurring," JOSA A, **19**, 1286-1296, (2002).
9. J. Goodman, "*Introduction of Fourier Optics*" (Mc-Graw Hill, New York, 1996).
10. M. Born and E. Wolf, "*Principles of Optics: Electromagnetic theory of propogation, inteference and diffraction*" (Cambridge University Press, 1999).
11. E. R. Dowski and W. T. Cathey, "Extended depth of field through wavefront coding," Appl. Opt., **34**, 1859-1866 (1995).
12. T. Cover and J. Thomas, "*Elements of Information Theory*" (John Wiley and Sons, New York, 1991).

1. Introduction

Imaging systems are often designed with the aim of achieving "good visual quality." Such a design metric is appropriate for applications such as photography and image display. In many

#2667 - $15.00 US Received July 01, 2003; Revised August 06, 2003

modern applications such as information storage, surveillance, communications and pattern recognition, visual quality plays no direct role. In these applications the design goal may be cast in the form of information-based metrics such as bit error rate, channel capacity, and/or reliability. This information-based approach to the design and analysis of imaging systems is gaining the attention of many researches [1],[2],[3],[4], [5],[6],[7],[8]. A majority of the cited literature assumes a Gaussian source model as was introduced in [6]. This model has the advantage that a closed-form analytic expression for information-density can be obtained. It has been used extensively in [1], [2], [3] and [7] to study the performance of various types of imagers. However, we should note that the Gaussian source model is not applicable to all imaging systems, e.g., the imager studied in [4] uses a binary source model. The present paper adopts a similar model. We consider a source space comprising relatively few equal-intensity point sources and we describe an information-based analysis of several systems used to image such a space. We take a somewhat unusual perspective in which the goal of each imager is not to directly measure a "pretty picture" but rather to extract the maximum possible scene information. We note that whenever all of the scene information has been extracted, an arbitrarily precise reconstruction of the scene is possible.

Here we define the information capacity of an imaging system as the mutual information between the object space and the measurement space. We refer to this quantity as the imaging mutual information (IMI) and use it as a metric to analyze the performance of three candidate systems: 1) a conventional lens imager, 2) a cubic phase mask imager and 3) a random phase mask imager. Each of these candidate systems is evaluated in three separate measurement configurations: 1) single detector, 2) two detectors in a single aperture and 3) one detector in each of two apertures. Because the object space has significant extent along the optical axis, both axial and lateral information are computed separately for each imaging system. The total information is also computed and is compared as a function of various physical variables.

2. Imaging system layout

Consider a scene comprising relatively few (one to six) equal-intensity monochromatic ($\lambda = 500nm$) point sources located within a source volume whose axial and lateral extents are both L as shown in Fig. 1(a). The conventional lens system layout shown in Fig. 1(a), contains a single lens of focal length f followed by an aperture stop of size D. The ideal object plane is located at the center of the source volume indicated by object distance S_o. The corresponding image plane is located at a distance S_i behind the imaging lens and contains up to two detectors parameterized by their sizes d_1,d_2 and positions h_1,h_2. Note that the analysis of this volumetric imaging system is restricted to two dimensions for reasons of computational simplicity.

The distributed aperture imaging system uses two apertures as shown in Fig. 1(b). The second aperture is positioned at an angle θ with respect to the optical axis of the first aperture. Here both apertures are identical in the sense that they both use lenses with the same focal length f and aperture stop D. The object and image distances for both apertures are also equal. Each aperture in our distributed imaging system contains only one detector. The imaging systems in this study are simulated using a diffraction-based shift-invariant image formation model. The model computes the point spread function (PSF) of the system using the Fresnel diffraction integral [9]. Defocus is also incorporated into the calculation of the PSF for off-focus point source positions [10]. The detector intensity for each point source position is computed by integrating the optical field over the detector area.

In addition to the single-lens system described above, we study systems with cubic and random phase masks. Whereas the aperture stop of the conventional system is clear, the cubic phase mask system uses a rectangularly separable cubic phase mask in this aperture stop [11]. The cubic phase mask extends the depth of the field of the system as compared to the conventional

#2667 - $15.00 US Received July 01, 2003; Revised August 06, 2003

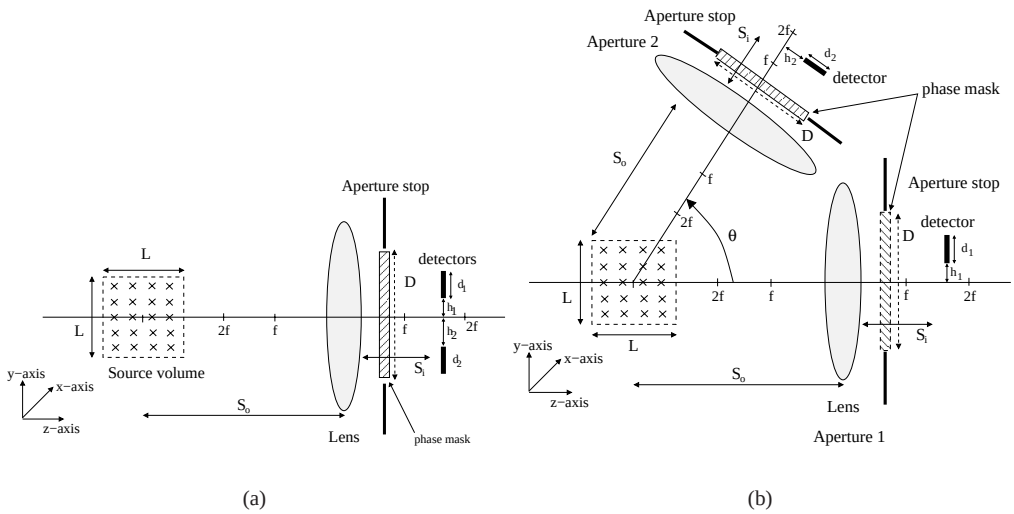

Fig. 1. Imaging system layout: (a) Single aperture system (b) Distributed aperture system.

lens system. The cubic phase mask is defined as $\phi(x,y) = \alpha \cdot (x^3 + y^3)$ where ϕ is the phase at position (x,y) [11]. The parameter α controls the depth of field of the system. Figure 2(a) shows a cubic phase profile with $\alpha = 30$. In this paper, we set $\alpha = 120$ such that the extended depth of field of the imaging system covers the entire axial extent of the source volume. Note that the PSF of a cubic phase mask system is significantly broader than the *Airy* PSF of a conventional lens system. For example, the PSF of a conventional lens system with a $f/2$ lens, measures only 10μm in comparison to a 1700μm wide PSF of the cubic phase mask system with $\alpha = 120$.

The random phase mask imaging system employs a random phase mask in the square aperture stop of the conventional lens system. The random phase mask is parameterized by roughness δ, spatial correlation length ρ and mean thickness Δ. The phase mask is designed using the following method: 1) independent uniformly distributed random numbers are generated from the interval [-δ,+δ] for every point (x,y) (phase mask is generated on a discrete grid) 2) these random numbers are filtered with a Gaussian filter of width/height ρ to obtain the phase $\phi(x,y)$ and 3) a constant Δ is added to phase $\phi(x,y)$ to give the phase mask an average thickness of Δ. As a result of the filtering, the phase variations have a correlation length of ρ. Figure 2(b) shows an example of a random phase profile with δ=800μm, ρ=18.7mm and Δ=200μm. The use of a random phase mask (δ=1200μm, ρ=3.6mm and Δ=200μm) results in a PSF whose extent is 2730μm for a $f/2$ lens. The width of the PSF is one of the important factors in this paper as it directly affects the optical power detected by a detector. Consider a detector located on the optical axis behind the lens. As a point source moves away from the optical axis in the source volume, the PSF moves off the detector center. For a PSF with a small width (relative to the detector size) the detected optical power decays to zero quickly as the point source moves off the optical axis. However, for a PSF with larger extent, the detected optical power changes slowly as the larger diffraction pattern slides across the detector due to the movement of point source away from the optical axis. Thus, a wider PSF results in a relatively large number of non-zero detector measurements as opposed to a PSF with a small width.

3. Information theoretic approach

In general, the goal of a task-specific imaging system is to acquire specific information about the scene. This paper treats a constrained source space for which any scene can be completely

#2667 - $15.00 US Received July 01, 2003; Revised August 06, 2003

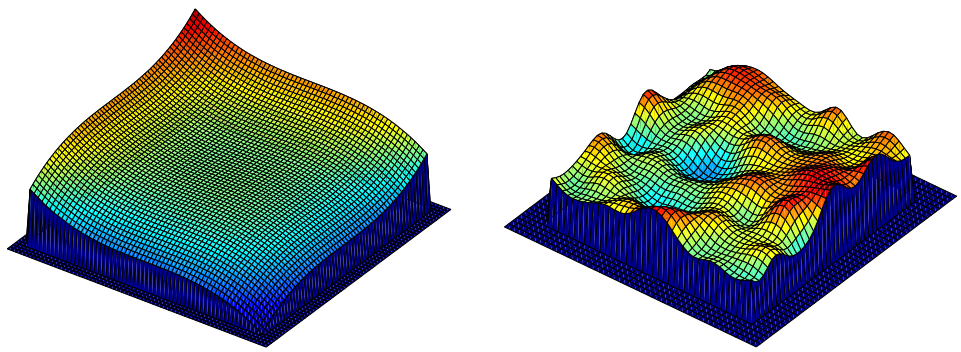

(a) (b)

Fig. 2. (a) Cubic phase profile and (b) Random phase profile.

described by the axial(z) and lateral(y) positions of each equal-intensity point source in the source volume. The optical power collected on each detector (I_r) in the imaging system serves as a measurement of the scene and is assumed to be corrupted by additive white Gaussian noise N. Therefore, the measured image data (I_{rn}) can be expressed as: $I_{rn} = I_r + N$. The performance of an imaging system can be characterized in terms of how much desired scene information is conveyed by the measured image data. Thus, if the information content of the measured image data (I_{rn}) and the scene S is quantified in terms of their respective Shannon entropies $h(I_{rn})$ and $h(S)$, then the imaging mutual information (IMI) between the scene and the image data can be used as a measure of the imaging system performance [4],[8]. By definition, IMI is upper bounded by the source entropy $h(S)$ because we can not hope to extract more information than what is available in the scene. Therefore, a IMI equal to $h(S)$ implies that we can completely reconstruct the scene from the measured image data. Mathematically, the IMI $I(I_{rn};S)$ can be expressed as $I(I_{rn};S) = h(I_{rn}) - h(I_{rn}|S)$, where $h(I_{rn}|S)$ is the conditional entropy of image data given the scene [12]. Under the independent additive noise assumption the IMI expression simplifies to $I(I_{rn};S) = h(I_{rn}) - h(N)$. For the purposes of computing IMI, the scene volume is quantized into a 128×128 square grid of allowed source positions. The total information in the source space is therefore $h(S) = log_2 \binom{16,384}{M}$, where M is the number of point sources in the scene. For a single point source: M=1 and h(S)=14bits. The use of a quantized source space allows us to estimate the IMI using discrete entropies as $I(I_{rn};S) \approx H(I_{rn}) - H(N)$, where $H(I_{rn})$ and $H(N)$ are the discrete counterparts of $h(I_{rn})$ and $h(N)$ respectively. Note that calculating IMI involves computing both $H(I_{rn})$ and $H(N)$. The latter entropy is easily calculated as it depends only on the noise power (σ^2) and is given as h(N)=$\frac{1}{2} log_2(2\pi e \sigma^2)$. The estimation of $H(I_{rn})$ is more challenging as it depends on the specific optical system under study. Here, $H(I_{rn})$ is estimated using the following exhaustive method: (1) consider all possible configurations of point sources in the source space, (2) for each such configuration simulate the imaging system using the diffraction-based model described earlier, (3) from each optical system simulation obtain the optical power I_r collected at each detector, (4) using values of I_r resulting from all $\binom{16,384}{M}$ configurations, estimate the probability density function (pdf) of I_r and convolve it with the pdf of the noise to obtain an estimate the measurement (I_{rn}) pdf and (5) compute $H(I_{rn})$

#2667 - $15.00 US Received July 01, 2003; Revised August 06, 2003

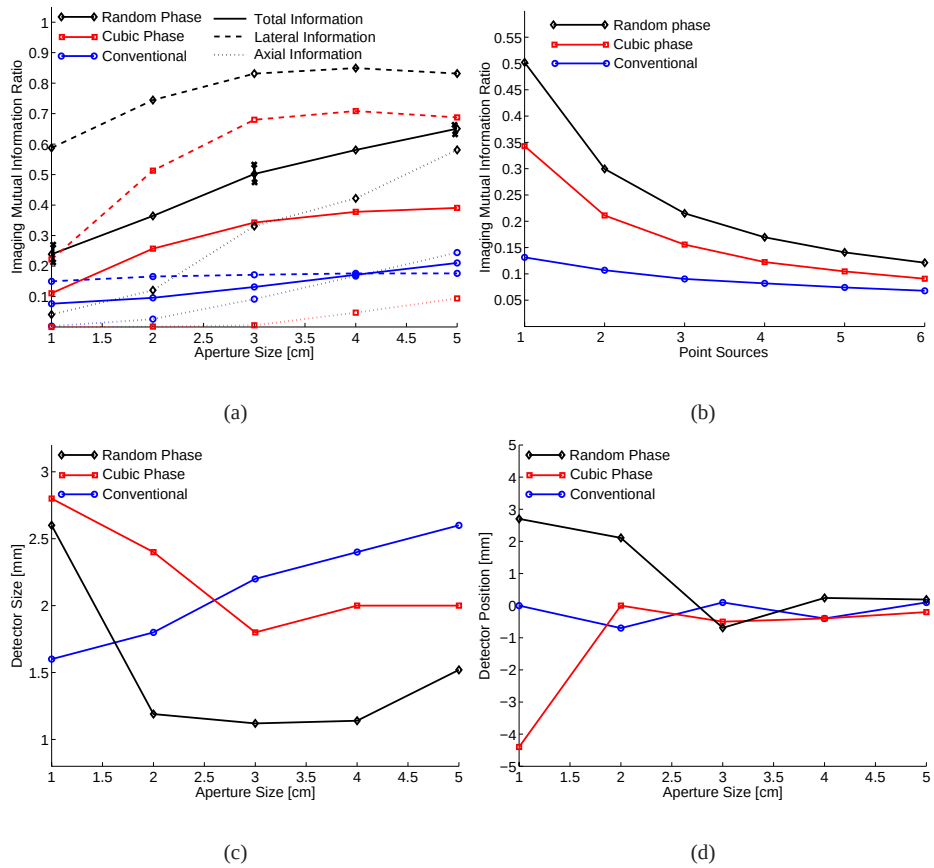

Fig. 3. Single detector imager (a) Total/axial/lateral IMI ratio (b) Total IMI ratio for multiple point sources with (D=3cm) (c) Optimal detector size and (d) Optimal detector position.

as the entropy of the measurement pdf. This procedure is repeated for all values of d_1, d_2, h_1 and h_2 to find the optimal detector sizes and positions. Although, the IMI value is instructive as a relative performance metric, the IMI ratio $\left(\frac{IMI}{h(S)}\right)$ is an absolute metric which is always strictly ≤ 1. Note that all IMI results presented in the paper are obtained for optimized detector size(s) and position(s).

4. A single detector in a single aperture

In this section, the IMI estimation method described earlier is applied to compute the information capacity of several single detector imagers. The imaging systems studied here use a lens of focal length f=10cm, an object distance of S_o=40cm and a source space defined by L=1cm. All sources have power P_{src}=0.5mW. The detector noise equivalent power is set to N_{ep}=2nW. In the cubic and random phase mask imagers, the cubic phase mask is defined by α=120 and the random phase mask parameters are: $\delta = 1200\mu$m, $\rho = 3.6$mm and $\Delta = 200\mu$m. First, consider a single point source in the source space. Figure 3(a) shows a plot of the axial, lateral and total IMI ratio for all three systems as a function of aperture size. This data shows that the total IMI ratio increases with aperture size. The main reason for this is the increased light collection ability of larger apertures which in turn improves the signal to noise ratio of the measured image

#2667 - $15.00 US Received July 01, 2003; Revised August 06, 2003

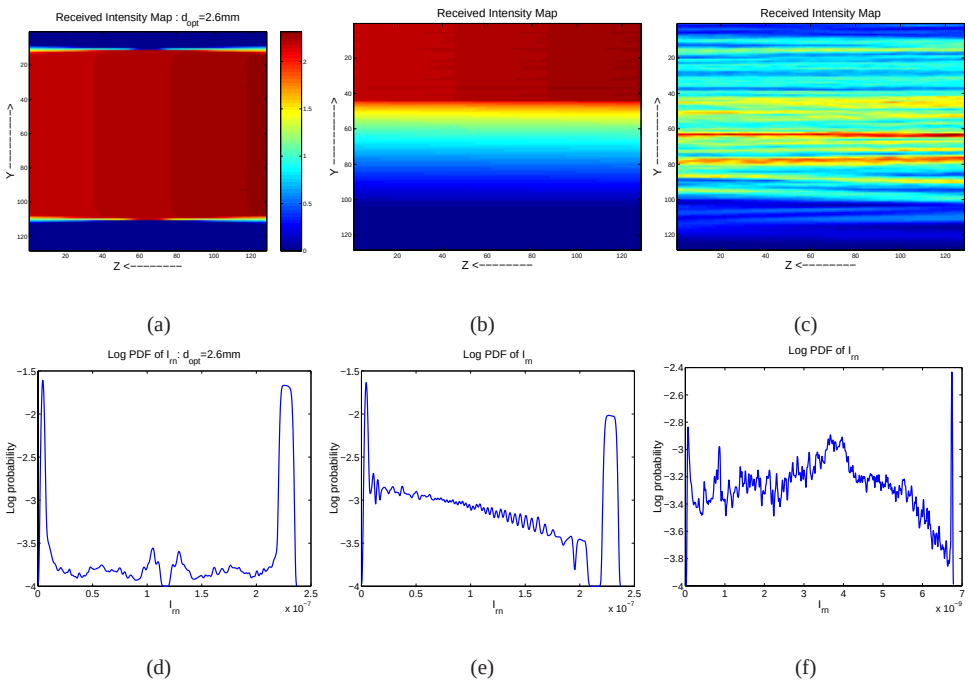

Fig. 4. Detector intensity maps (a), (b) and (c) and detector intensity log-pdf (d), (e) and (f) for conventional lens, cubic phase mask and random phase imagers respectively with D=3cm.

data. Note that the random phase mask imager's total IMI ratio depends on the sample realization of the random phase mask. This is shown in Fig. 3(a) by means of error bars based on 10 trials at D=1cm, 3cm and 5cm apertures. Less than 8% variation in total IMI ratio is observed.

We can see from Fig. 3(a) that the conventional lens system offers the least total information, peaking at 21% for an aperture of 5cm ($f/2$ lens). In contrast, the cubic phase mask imager offers a higher total IMI ratio of almost 39%. It is interesting to note that the cubic phase mask system suffers from a loss of axial information due to its extended depth of field. However, a large increase in lateral information, compared to that of a conventional lens imager, results in an overall higher total IMI ratio. This increase in lateral information is due to the larger lateral extent of its PSF. This dependence can be understood by considering the intensity maps in Fig. 4(a) and Fig. 4(b). The intensity map represents the intensity measured by a detector for every point source position in the discretized source volume. The intensity map is used to generate the pdf of the intensity I_{rn} as measured by the detector. Figure 4(d) and Fig. 4(e) show the corresponding pdf for the intensity maps in Fig. 4(a) and Fig. 4(b). The large variation in the intensity map of the cubic phase system, shown in Fig. 4(b), results in a more uniform pdf of the measured detector intensity compare to the conventional lens system. Note that the entropy of the measured detector intensity and therefore the IMI, is directly related to the uniformity of the pdf. Hence, the cubic phase system achieves a higher IMI ratio. The random phase mask imager achieves the highest total IMI ratio of nearly 65% as shown in Fig. 3(a). This is due to the relatively uniform distribution of light across the image plane as shown by its intensity map in Fig. 4(c). This distribution of light results in even a more uniform pdf (Fig. 4(f)) and therefore the largest total IMI ratio. Note that these results may first appear to be counter-intuitive since a larger PSF is traditionally associated with degradation of imaging system performance.

#2667 - $15.00 US
Received July 01, 2003; Revised August 06, 2003

However, the goal of the imager considered here is to estimate the position of each equal-intensity point source in the constrained source volume. Therefore, the imaging performance is directly related to the IMI ratio. As mentioned above a larger PSF gives the intensity pdf more uniformity which effectively increases the IMI ratio. It is also important to note that it is not only the extent of PSF but also the resulting diversity of measurements which contributes to the uniformity of the intensity pdf.

Figure 3(b) shows a plot of the total IMI ratio for all three imagers with a $f/3.3$ lens as a function of the number of point sources in the source volume. Although the total IMI value increases with M, the IMI ratio decreases with M due to the much faster increase in source entropy. Figure 3(b) demonstrates that the random and cubic phase mask imagers can provide much greater source information than a conventional lens for small M. Figures 3(c) and (d) show the optimized detector sizes and positions for each imager as a function of aperture size. Note that the detector size for the random phase mask imager is nearly an order of magnitude smaller than that of the conventional and cubic phase mask imagers. The relatively small scale of the received intensity variations shown in Fig. 4(c), due to the actual shape of the random phase mask PSF that drives the detector to a smaller size.

5. Two detectors in a single aperture

This configuration utilizes two detectors in the image plane as shown in Fig. 1(a). Note that all other system parameters remain unchanged from the single detector configuration. We expect that the two detector imager will offer higher IMI ratios relative to the single detector imager for two reasons: 1) higher lateral sensitivity and 2) more collected optical power. To understand how the two detector configuration improves the effective signal to noise ratio consider a limiting case in which the two measurements are identical and equal to the measurement obtained in the case of a single detector. In this case the two measurements could be simply averaged to improve the overall SNR, thus increasing total IMI. This improvement is confirmed by the plots of the axial, lateral and total IMI ratios shown in Fig. 5(a). Once again this data is generated using a single point source in the source volume. The total IMI ratio plot shows that the conventional lens imager offers a total IMI ratio of about 30%, only a 9% improvement from the single detector case. This improvement is mainly due to an increase in lateral IMI ratio from 18% in the single detector case to 33% in the two detector case. The cubic phase mask imager demonstrates similar improvements in total and lateral IMI ratios, increasing from 39% and 69% in the single detector case to 54% and 94% respectively in the two detector configuration. The random phase mask system achieves the highest total IMI ratio of nearly 74% as shown in Fig. 5(a). The lateral IMI ratio saturates at nearly 85% and the axial IMI ratio increases from 58% for a single detector to 64% for two detectors.

Figure 5(b) shows the total IMI ratio of the three imagers with a $f/3.3$ lens for multiple point sources. Note that the IMI ratio has increased relative to the single detector case. Because some point source positions contribute optical power to both detectors, the two intensity measurements are not strictly independent. As a result, the total IMI ratio is not exactly double that of the single detector results. This implies that total IMI would increase as number of detectors are increased. However, we should note that the total IMI is upper bounded and thus will always be strictly less than 1.0 for any number of detectors. Figures 5(c) and (d) show the optimized detector sizes and positions for all three imagers as a function of aperture size. Note that the optimal size of each of the two detectors is smaller than the detector of the corresponding single detector imager. This smaller detector size affords more information in each imager as evident from all three IMI ratio values. Again, the random phase mask imager has the smallest detectors due to the relatively small scale of variations in the random phase mask PSF.

#2667 - $15.00 US Received July 01, 2003; Revised August 06, 2003

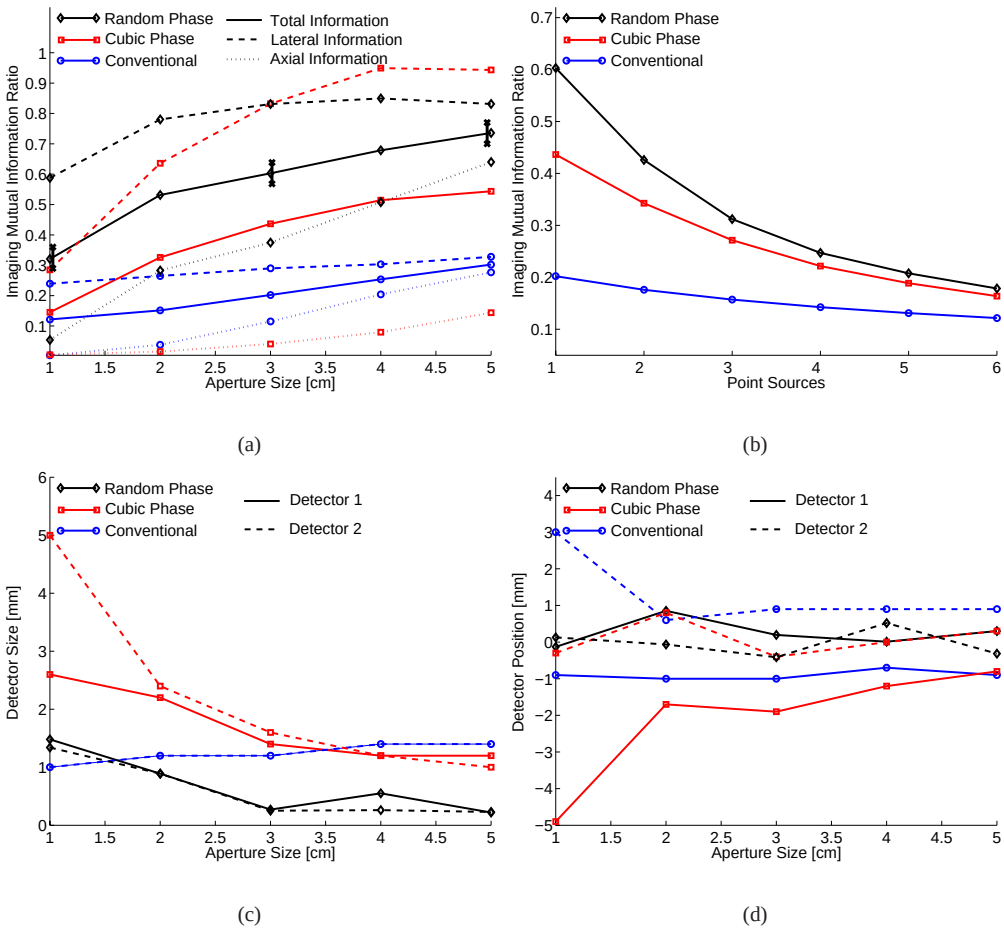

Fig. 5. Single aperture two detector imager (a) Total/axial/lateral IMI ratio (b) Total IMI ratio for multiple point sources with (D=3cm) (c) Optimal detector sizes and (d) Optimal detector positions.

6. One detector in each of two apertures

Consider the two aperture imager shown in Fig. 1(b). Once again, all system parameters remain unchanged with the exception of the new variable θ which is varied in the range of 15° to 90°. The lateral, axial and total IMI ratios are computed for the three imagers and tabulated in Table 1 for D=3cm. The IMI values show that both axial and total IMI ratios increase with angle θ. This is due to the fact that the lateral direction in the second aperture has some projection along the axial direction of the first aperture. Therefore, the lateral discrimination of the second aperture effectively improves the overall axial sensitivity relative to the single aperture imager. An exception to this trend is observed in the case of the conventional lens imager, for which the axial information actually decreases at angles near 45°. This is due to the symmetry in the PSF that results in symmetric detector intensity measurements at angles close to 45° which effectively reduces the axial and the total IMI.

Figure 6(a) shows a plot of the lateral, axial and total IMI ratios of all three imagers with $\theta = 90^o$. As in previous configurations, the random phase imager offers the highest total IMI ratio of 89.3%. The axial IMI ratio improves from 58% in the single aperture case to 85.6%

#2667 - $15.00 US
Received July 01, 2003; Revised August 06, 2003

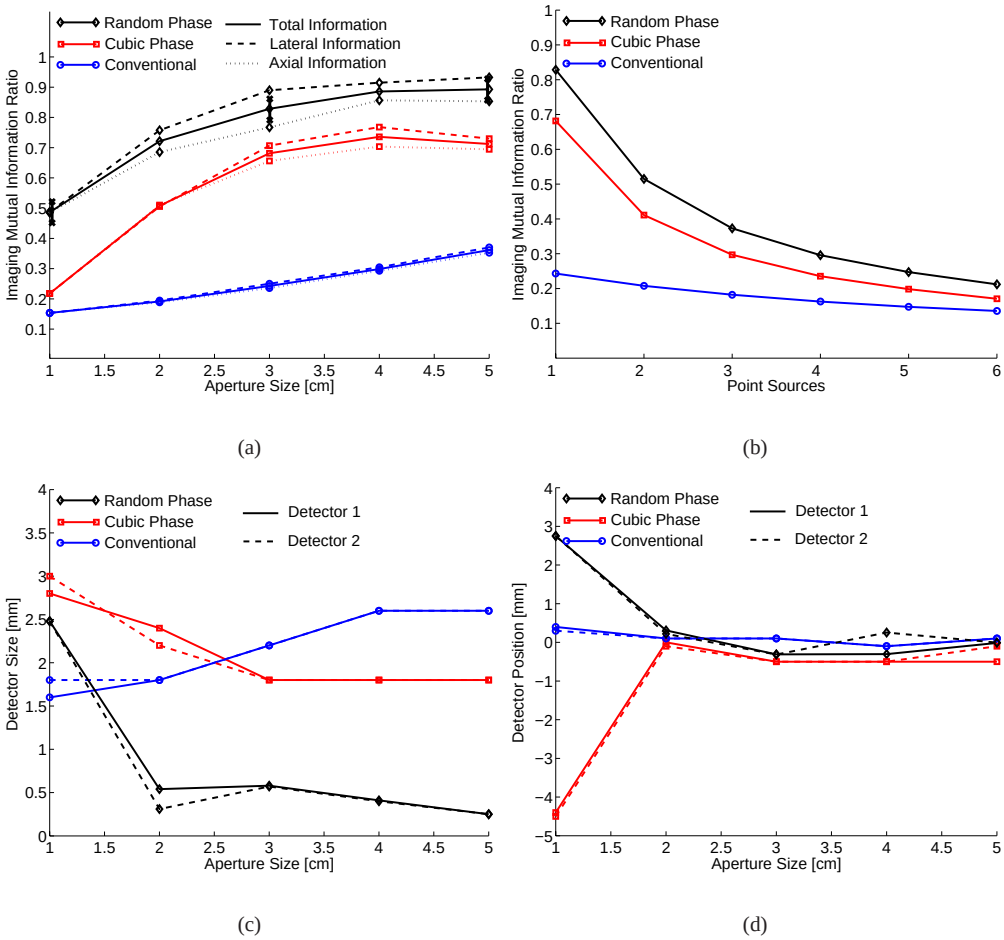

Fig. 6. Distributed aperture two detector imager (a) Total/axial/lateral IMI ratio for single point source (b) Total IMI ratio for multiple point sources (D=3cm) (c) Optimal detector sizes and (d) Optimal detector positions ($\theta = 90^o$).

in the present configuration due to added axial sensitivity. The cubic phase imager follows with a total IMI ratio of 73.6% with nearly 70.3% axial IMI ratio. Conventional lens imaging also shows substantial improvement from a total IMI ratio of 21% for the single aperture case to 36% in the present case. In the case of multiple point sources the total IMI ratio shows a similar trend to those observed in the previous two configurations. Figures 6(c) and (d) show the optimized detector sizes and positions for all three imagers as a function of aperture size. As mentioned before, all IMI ratio values were obtained for optimized detector size and position that maximize the information. We have found that the gradients of the total IMI surface are quite small. Small perturbations in detector size and positions from their optimal values resulted in only small changes in the total IMI value. Departure from optimality along any one direction i.e. either size or position by approximately 10% resulted in a total IMI loss of less than 5%.

#2667 - $15.00 US
Received July 01, 2003; Revised August 06, 2003

Table 1. Total/axial/lateral IMI ratio of three imagers for various angles (D=3cm).

Imager Type	θ[deg]	15	30	45	60	75	90
Random Phase Mask Imager	Total IMI ratio	77.9%	80.0%	80.7%	81.4%	82.9%	82.9%
	Lateral IMI ratio	97.8%	98.4%	98.2%	97.3%	96.8%	89.0%
	Axial IMI ratio	57.9%	61.6%	63.3%	65.6%	68.9%	76.7%
Cubic Phase Mask Imager	Total IMI ratio	61.0%	64.9%	66.1%	67.1%	67.8%	68.1%
	Lateral IMI ratio	85.0%	84.3%	82.7%	81.4%	79.1%	70.7%
	Axial IMI ratio	37.0%	45.5%	49.6%	52.8%	56.4%	65.6%
Conventional Lens Imager	Total IMI ratio	25.0%	24.1%	24.7%	25.1%	24.7%	24.3%
	Lateral IMI ratio	34.1%	32.2%	33.1%	32.0%	30.0%	25.1%
	Axial IMI ratio	15.9%	15.9%	16.3%	18.1%	19.4%	23.4%

7. Conclusions

The information-based analysis presented here offers insight into the various mechanisms that influence the information capacity of a simple imaging system. It is observed that modifications to a conventional lens system using simple phase masks can result in a substantial improvement in information capacity. For example, with a single point source, the random phase mask imager achieves a total IMI ratio of 65% which is three times that offered by the conventional lens imager in the single detector configuration. Doubling the number of detectors increases the total IMI ratio of the random phase mask imager to nearly 74% for a single aperture or 89% with two apertures. These information capacity results suggest that it is not always necessary to make a large number of measurements to achieve good imaging performance. The distributed imager results show that a large fraction of the scene information can be obtained with only two detectors for a constrained source volume. The information-based analysis also highlights an important relationship between the size of PSF and the imaging performance. The results reported here show that a wider PSF does not necessarily imply loss of information in an imager, as predicted for traditional imagers. The cubic phase mask system proposed in [11] has in fact a larger optical PSF extent compare to an equivalent conventional lens imaging system but offers a relatively higher lateral resolution over an extended depth of field as compared to a conventional lens imager.

The current approach for IMI calculation is computationally intractable for a detector plane consisting of many elements. Also, the source space is assumed to be two dimensional, that could be extended to three dimensions. We are currently working on methods of managing this computational complexity while obtaining good approximate results.

#2667 - $15.00 US Received July 01, 2003; Revised August 06, 2003